A non-second-gradient model of nonlinear electro-elastic bodies with fibre stiffness

M.H.B.M. Shariff[1], J. Merodio[2], R. Bustamante[3], A. Laadhari[1]

[1] Department of Mathematics

Khalifa University of Science and Technology, UAE.

[2] Departamento de Matemtica Aplicada a las TIC, ETS de Ingeniera de Sistemas Informticos

Universidad Politcnica de Madrid, Madrid, 28031, Spain

[3] Departamento de Ingeniería Mecánica, Universidad de Chile

Beauchef 851, Santiago Centro, Santiago, Chile.

Abstract

The study of the mechanical behaviour of fibre-reinforced electro-active polymers (EAPs) with bending stiffness is beneficial in engineering for mechanical design and problem solving. However, constitutive models of fibre-reinforced EAPs with fibre bending stiffness do not exist in the literature. Hence, to enhance the understanding of the mechanical behaviour of fibre-reinforced EAPs with fibre bending stiffness, the development of a relevant constitutive equation is paramount. In this paper, we develop a constitutive equation for a non-linear non-polar EAP, reinforced by embedded fibres, in which the elastic resistance of the fibers to bending is modeled via the classical branches of continuum mechanics without using the second gradient theory, which assumes the existence of contact torques. In view of this, the proposed model is simple and somewhat more realistic, in the sense that contact torques do not exist in non-polar EAPs.

Keywords: fibre-reinforced electro-active polymers, bending stiffness, spectral invariant, non-polar, hyperelasticity

1 Introduction

Recent research in various fields of science and engineering has led to the development of new materials and technologies. For instance, the effect of dielectric relaxation of epoxy resin on the dielectric loss of medium-frequency transformer was investigated in [45]. In [10], a novel one-dimensional V3S4@NC nanofibers for sodium-ion batteries was proposed. Meanwhile, the physical layer security of uplink NOMA via energy harvesting jammers was improved in [2]. In another study, the structures and stabilities of carbon chain clusters influenced by atomic antimony was examined in [41]. Furthermore, Shi et al. integrated redox-active polymer with MXene for ultra-stable and fast aqueous proton storage [39]. In [46], an analytical model for the nonlinear buckling responses of confined polyhedral FGP-GPLs lining subjected to crown point loading in engineering structures was developed.

In this paper, we are interested in the mechanical behavior of fibre-reinforced electro-active polymers (EAPs) with bending stiffness, which is an important issue in engineering. EAPs are multifunctional materials that are innovative and smart as they can adapt their physical and mechanical properties as a result of external stimuli. An EAP deforms under the application of an electric field and it has recently attracted growing interest because of its potential for use, for example, in biomedical applications, artificial muscles in robotics and actuators [1].

Fibre-reinforced composite materials have often been used in recent engineering applications. The rapid growth in manufacturing industries has led to the need for the improvement of materials in terms of strength, stiffness, density, and lower cost with improved sustainability. Fibre-reinforced composite materials have emerged as one of the materials possessing such improvement in properties serving their potential in a variety of applications [3, 15, 38, 47]. The infusion of natural synthetic or natural fibers in the fabrication of composite materials has revealed significant applications in a variety of fields such as biomedical, automobile, mechanical, construction, marine and aerospace [4, 18, 20, 48]. In biomechanics, some soft tissues can be modelled as fibre-reinforced composite materials [7, 25, 27]. In modern heavy engineering, the heavy traditional materials are gradually being replaced by fibre-reinforced polymer composite structures of lower weight and higher strength. These structures, such as railroads and bridges, are always under the action of dynamic moving loads caused by the moving vehicular traffic.

Constitutive equations for fibre-reinforced EAPs have recently been developed [29, 30]. However, fibre-reinforced EAP models that appear in the literature do not consider fibres that resist bending. Hence, the understanding of the mechanics of fibre-reinforced EAPs, where the fibres resist bending is an important issue in engineering. The mechanical behavior of fibre-reinforced EAPs with stiff bending fibres is significantly different from those that are perfectly flexible [6]. Hence, in view of the above, a rigorous construction of a mechanical constitutive model, based on the sound theory of continuum mechanics, for non-polar fibre-reinforced solids, is paramount, and is of valuable interest in engineering designs and would find many practical applications.

In the case of non-EAP materials, the long history [24, 28, 43] of mechanics of *non-polar* fiber-reinforced solids has, in general, significantly enriched and advanced the knowledge of solid mechanics. A boundary value problem for a non-polar elastic solid reinforced by (*finite radius*) fibres can be solved using the Finite Element Method (FEM), if small elements are permittable to mesh the fibres. If we treat the fibres to be an isotropic solid but have a different material properties from the matrix (material that is not attributable to the fibers) properties, we can use an inhomogeneous strain energy function

$$W(\lambda_1, \lambda_2, \lambda_3) \tag{1}$$

in solving the FEM problem, where λ_1, λ_2 and λ_3 are the pricipal stretches. We note that, due to the finite radius of the fibres, bending resistance due to changes in the curvature for the fibres, is observed. However, if the fibre radius is significantly small, meshing the fibres and the matrix can be troublesome and hence it may not be possible to seek a boundary value solution via the FEM. To overcome this significantly small radius problem, a FEM solution can be obtained using a transversely elastic strain energy function [43]

$$W(\boldsymbol{U}, \boldsymbol{a})\,, \tag{2}$$

where $\boldsymbol{U}$ is the right-stretch tensor and $\boldsymbol{a}$ is the unit preferred vector in the reference configuration. We note that this transversely isotropic model contains infinitely many purely flexible fibres with zero radius; hence this model cannot model elastic resistance due to changes in the curvature for the fibres. We emphasize that the Cauchy stress in both isotropic and transversely isotropic non-EAP models is symmetric and this is actually observed in a non-polar solid in the absence of a couple stress. To model the effect of elastic resistance due to changes in the curvature for the fibres, recent models [32, 33, 40, 42] that are framed in the setting of the non-linear strain-gradient theory or Kirchhoff rod theory [44], were developed. We note that these second-gradient models characterize the mechanical behaviour of (polar) transversely isotropic solids with infinitely many purely flexible fibres with zero radius. But, in order to simulate the effect of fibre bending stiffness on purely flexible fibres with zero radius, the second-gradient non-EAP models introduce the existence of a couple stress and a non-symmetric Cauchy stress in the constitutive equations; we must emphasize that both of these stresses are not present on deformations of actual non-polar-EAP elastic solids reinforced by finite-radius fibres. In general, higher gradient elasticity models are used to describe mechanical structures at the micro-and nano-scale or to regularize certain ill-posed problems by means of these higher gradient contributions. Discussion on the effectiveness of higher gradient elasticity models to mechanically describe continuum solids is still ongoing [8, 9, 21].

Hence, the objective of this paper is to propose a model to simulate the mechanical behaviour of actual non-polar EAP reinforced by finite- radius fibres, where the contact torque is absent and fibre bending resistance

is caused by changes in curvature of the fibres. We focus on changes in fibre curvature, since in composite solids, these changes play an important role in the mechanical behaviour of solids. Since our simulated model contains infinitely many fibres with zero radius, we exclude the effects due to fibre 'twist'. In fact Spencer and Soldatos [42] stated that
"In doing this, we exclude effects due to fibre 'splay' and fibre 'twist', both of which feature in liquid crystal theory, but it is plausible that in fibre composite solids the major factor is fibre curvature."

Please note that our model does not:
(1) Require the existence of contact torques (which are not observed in actual non-polar elastic solids reinforced by finite-radius fibres).
(2) Introduce higher order differential equations in the corresponding boundary value problem.
Both (1) and (2) complicate the solving of boundary value problems, which is discussed in references[8, 9, 21]. Since our model does not involve (1) and (2), solving EAP boundary value problems is much easier, analytically and numerically, compared to solving boundary value problems of second-gradient models that are asscociated with (1) and (2).

Spectral approach [31, 32] is used in the modelling and this is preliminary described in Sections 2 and 4, where in Section 4 a total energy function contains an electric field and a vector that governs the changes in the fibre curvature. A prototype of the strain energy is given in Section 5 and boundary value problems to study the effect of fibre bending resistance are presented in Section 6.

2 Preliminaries

2.1 Deformation

Unless stated otherwise, all subscripts i, j and k assume the values of 1 or 2 or 3 and we do not use the summation convention. Let $\boldsymbol{y}$ and $\boldsymbol{x}$ denote the position vectors of a solid body particle, respectively, in the current and reference configurations. The deformation gradient $\boldsymbol{F}$ is spectrally [28] described as follows:

$$\boldsymbol{F}(\lambda_i, \boldsymbol{v}_i, \boldsymbol{u}_i) = \frac{\partial \boldsymbol{y}}{\partial \boldsymbol{x}} = \sum_{i=1}^{3} \lambda_i \boldsymbol{v}_i \otimes \boldsymbol{u}_i \,, \tag{3}$$

where λ_i is a principal stretch, $\boldsymbol{u}_i$ is an eigenvector of the right- stretch tensor $\boldsymbol{U} = \boldsymbol{F}(\lambda_i, \boldsymbol{u}_i, \boldsymbol{u}_i)$ and $\boldsymbol{v}_i$ is an eigenvector of the left stretch tensor $\boldsymbol{V} = \boldsymbol{F}(\lambda_i, \boldsymbol{v}_i, \boldsymbol{v}_i)$. We can spectrally express the rotation tensor $\boldsymbol{R} = \boldsymbol{F}(\lambda_i = 1, \boldsymbol{v}_i, \boldsymbol{u}_i)$ and the right Cauchy-Green tensor $\boldsymbol{C} = \boldsymbol{F}(\lambda_i^2, \boldsymbol{u}_i, \boldsymbol{u}_i)$, where $\boldsymbol{F} = \boldsymbol{R}\boldsymbol{U}$. In this article, we assume that the effect of mechanical body forces is negligible and only incompressible elastic solids are considered. Hence, $\det \boldsymbol{F} = 1$, where $\det$ indicates the tensor determinant. We only consider time-independent fields and quasi-static deformations.

2.2 Electrostatics

In the absence of distribution of free charges the simplified forms of the Maxwell equations are [36]

$$\mathrm{div}(\boldsymbol{d}) = 0 \,, \quad \mathrm{curl}(\boldsymbol{e}) = 0 \,, \tag{4}$$

where $\boldsymbol{d}$ is the cuurent-configuration electric displacement, $\boldsymbol{e}$ is the current-configuration electric field and, curl and div are, respectively, the curl and divergence operators with respect to $\boldsymbol{y}$. The relation between $\boldsymbol{d}$ and $\boldsymbol{e}$ in vacuum is

$$\boldsymbol{d} = \varepsilon_0 \boldsymbol{e} \,, \tag{5}$$

where $\varepsilon_0 = 8.85 \times 10^{-12}$F/m is the vacuum electric permittivity. The condensed matter relation is

$$\boldsymbol{d} = \varepsilon_0 \boldsymbol{e} + \boldsymbol{p} \,, \tag{6}$$

where $\boldsymbol{p}$ is the electric polarization.

Let $\boldsymbol{T}$ be the total symmetric Cauchy stress defined in [5]. We assume surface electric charges are absent and hence, we have, the continuity equations [11, 23]

$$\boldsymbol{n}\cdot[\![\boldsymbol{d}]\!]=0,\quad \boldsymbol{n}\times[\![\boldsymbol{e}]\!]=\boldsymbol{0},\quad \boldsymbol{T}\boldsymbol{n}=\hat{\boldsymbol{t}}+\boldsymbol{T}_{\mathrm{M}}\boldsymbol{n}, \tag{7}$$

where $\boldsymbol{n}$ is the unit outward normal vector to the boundary of the deformed body, $\hat{\boldsymbol{t}}$ is the external mechanical traction, $[\![\ \ ]\!]$ denotes the difference of a quantity from outside and inside a body and $\boldsymbol{T}_{\mathrm{M}}$ is the Maxwell stress tensor outside the body in vacuum defined as

$$\boldsymbol{T}_{\mathrm{M}}=\boldsymbol{d}\otimes\boldsymbol{e}-\frac{1}{2}(\boldsymbol{d}\cdot\boldsymbol{e})\boldsymbol{I}. \tag{8}$$

3 Embedded fibres

We assume the material body consists of a matrix material and fibers. We model this material by considering a transversely elastic solid with the referential preferred unit direction $\boldsymbol{a}(\boldsymbol{x})$ and it becomes the vector

$$\boldsymbol{b}=\boldsymbol{F}\boldsymbol{a}=\varrho\boldsymbol{f}\,,\quad \varrho=\sqrt{\boldsymbol{a}\cdot\boldsymbol{C}\boldsymbol{a}}>0\,, \tag{9}$$

in the current configuration, where $\boldsymbol{f}$ is a unit vector. In our proposed model, the directional derivative of the fibre unit vector in the fibre direction, i.e.,

$$\boldsymbol{c}=\frac{\partial\boldsymbol{f}}{\partial\boldsymbol{x}}\boldsymbol{a}\,, \tag{10}$$

plays an important role in modelling elastic resistance due to changes in curvature for the fibres. In view of this we endow a vector $\boldsymbol{m}$ associated with $\boldsymbol{c}$ (we will make the association clear later) in (10), which is independent of $\boldsymbol{F}$, i.e. [32, 33, 37]

$$\boldsymbol{m}=\frac{1}{\iota}\boldsymbol{\Lambda}\boldsymbol{a}-\frac{1}{\iota^3}(\boldsymbol{a}\cdot\boldsymbol{\Lambda}\boldsymbol{a})\bar{\boldsymbol{C}}\boldsymbol{a}\,,\quad \iota=\sqrt{\boldsymbol{a}\cdot\bar{\boldsymbol{C}}\boldsymbol{a}}\,, \tag{11}$$

where

$$\bar{\boldsymbol{C}}=\bar{\boldsymbol{F}}^T\bar{\boldsymbol{F}}\,,\quad \boldsymbol{\Lambda}=\bar{\boldsymbol{F}}^T\boldsymbol{G}-\frac{\partial\boldsymbol{a}}{\partial\boldsymbol{x}}\,,\quad \boldsymbol{G}=\frac{\partial\bar{\boldsymbol{F}}\boldsymbol{a}}{\partial\boldsymbol{x}}\,, \tag{12}$$

$\bar{\boldsymbol{F}}(\boldsymbol{x})$ is the deformation tensor independent of $\boldsymbol{F}$, i.e., $\boldsymbol{m}$ is not embedded in the matrix, and so in general its image $\bar{\boldsymbol{F}}^{-T}\boldsymbol{m}$ in the current configuration is not directly connected to the deformation of the matrix. Clearly from (11), we have $\boldsymbol{m}\cdot\boldsymbol{a}=0$. If we let $\bar{\boldsymbol{F}}=\boldsymbol{F}$, we then have the association $\boldsymbol{c}=\boldsymbol{F}^{-T}\boldsymbol{m}$ [32, 33]. To facilitate the process of modelling, we express the vector

$$\boldsymbol{m}=\rho\boldsymbol{k}\,,\quad \rho=\sqrt{\boldsymbol{m}\cdot\boldsymbol{m}}\,, \tag{13}$$

where $\boldsymbol{k}$ is a unit vector with the property $\boldsymbol{a}\cdot\boldsymbol{k}=0$.

4 Total energy function

Let W be the total energy. Following the work of [5, 23], we have,

$$W=\hat{W}_{(a)}(\boldsymbol{U},\boldsymbol{a},\boldsymbol{m},\boldsymbol{e}_L)=W_{(a)}(\boldsymbol{U},\boldsymbol{a},\boldsymbol{k},\boldsymbol{g},\rho,e)\,, \tag{14}$$

where

$$\boldsymbol{g}=\frac{1}{e}\boldsymbol{e}_L\,,\quad e=|\boldsymbol{e}_L|>0\,. \tag{15}$$

and the Lagrangian electric field $\boldsymbol{e}_L$ is defined as $\boldsymbol{e}_L = \boldsymbol{F}^T\boldsymbol{e}$ [5].

For an incompressible body, the total symmetric Cauchy stress is [5]

$$\boldsymbol{T} = \boldsymbol{F}\frac{\partial\Omega}{\partial\boldsymbol{F}} - p\boldsymbol{I} = 2\boldsymbol{F}\frac{\partial\Omega}{\partial\boldsymbol{C}}\boldsymbol{F}^T - p\boldsymbol{I} \tag{16}$$

and the Eulerian electric displacement is

$$\boldsymbol{d} = -\boldsymbol{F}\frac{\partial\Omega}{\partial\boldsymbol{e}_L}\,. \tag{17}$$

The Lagrangian electric displacement is given as [5]

$$\boldsymbol{d}_L = -\frac{\partial\Omega}{\partial\boldsymbol{e}_L}\,, \tag{18}$$

where $\boldsymbol{d}_L = \boldsymbol{F}^{-1}\boldsymbol{d}$. The Lagrangian fields must satisfy the relations [5]

$$\mathrm{Curl}(\boldsymbol{e}_L) = \boldsymbol{0} \quad \text{and} \quad \mathrm{Div}(\boldsymbol{d}_L) = 0\,, \tag{19}$$

where Div and Curl are, respectively, the divergence and curl operators with respect to $\boldsymbol{x}$, associated with the undeformed configuration.

4.1 Spectral invariants

The total energy function requires the restriction

$$W = W_{(a)}(\boldsymbol{U}, \boldsymbol{a}, \boldsymbol{k}, \boldsymbol{g}, \rho, e) = W_{(a)}(\boldsymbol{Q}\boldsymbol{U}\boldsymbol{Q}^T, \boldsymbol{Q}\boldsymbol{a}, \boldsymbol{Q}\boldsymbol{k}, \boldsymbol{Q}\boldsymbol{g}, \rho, e)\,, \tag{20}$$

for every rotation tensor $\boldsymbol{Q}$, hence it must depend on invariants with respect to the rotation tensor $\boldsymbol{Q}$. Recently, attractive, useful and successful spectral invariants have been used in modelling anisotropic bodies (see for example references [25, 26, 28, 29, 30, 31, 32, 33]) and, in view of this, we characterise W by the spectral invariants [35]

$$\lambda_i \quad a_i = \boldsymbol{a}\cdot\boldsymbol{u}_i, \quad b_i = \boldsymbol{k}\cdot\boldsymbol{u}_i\,, \quad c_i = \boldsymbol{g}\cdot\boldsymbol{u}_i\,, \quad \sum_{i=1}^{3} a_i^2 = 1\,, \quad \sum_{i=1}^{3} b_i^2 = 1\,, \quad \sum_{i=1}^{3} c_i^2 = 1\,. \tag{21}$$

and the scalers ρ and e. Hence, we can express

$$W = W_{(a)}(\lambda_i, a_i, b_i, c_i, \rho, e)\,, \tag{22}$$

taking note the $W_{(a)}$ must satisfy the P-property described in [26] associated with the coalescence of principal stretches λ_i. In view of the 3 constraints in (21), only 11 of the invariants in (22) are independent; in the case of an incompressible material, only 10 of the invariants are independent due to the constraint $\lambda_1\lambda_2\lambda_3 = 1$. In our current model, W is independent of the sign of $\boldsymbol{a}, \boldsymbol{k}$ and $\boldsymbol{g}$, hence we express

$$W = W_{(s)}(\lambda_i, \alpha_i, \beta_i, \gamma_i, \rho, e)\,, \quad \alpha_i = a_i^2\,, \quad \beta_i = b_i^2\,, \quad \gamma_i = c_i^2\,. \tag{23}$$

4.2 Spectral derivative components

The evaluation of stress tensors requires spectral the Lagrangian spectral tensor components of $\dfrac{\partial W}{\partial\boldsymbol{C}}$ i.e.,

$$\left(\frac{\partial W}{\partial\boldsymbol{C}}\right)_{ii} = \frac{1}{2\lambda_i}\frac{\partial W_{(s)}}{\partial\lambda_i}\,, \tag{24}$$

$$\left(\frac{\partial W}{\partial \boldsymbol{C}}\right)_{ij} = \frac{1}{(\lambda_i^2 - \lambda_j^2)} \left\{ \left(\frac{\partial W_{(s)}}{\partial \alpha_i} - \frac{\partial W_{(s)}}{\partial \alpha_j}\right) a_i a_j + \left(\frac{\partial W_{(s)}}{\partial \beta_i} - \frac{\partial W_{(s)}}{\partial \beta_j}\right) b_i b_j + \left(\frac{\partial W_{(s)}}{\partial \gamma_i} - \frac{\partial W_{(s)}}{\partial \gamma_j}\right) c_i c_j \right\},$$

$$i \neq j\,. \tag{25}$$

The Eulerian description of the total Cauchy stress $\boldsymbol{T}$ for an incompressible body is

$$\boldsymbol{T} = \sum_{i,j=1}^{3} t_{ij} \boldsymbol{v}_i \otimes \boldsymbol{v}_j\,, \tag{26}$$

where

$$\tau_{ii} = \lambda_i \frac{\partial W_{(s)}}{\partial \lambda_i} - p\,, \quad \tau_{ij} = 2\lambda_i \lambda_j \left(\frac{\partial W}{\partial \boldsymbol{C}}\right)_{ij}\,, \quad i \neq j\,. \tag{27}$$

The Lagrangian spectral components for the electric displacement $\boldsymbol{d}$ are:

$$\boldsymbol{d}_L = -\frac{\partial W}{\partial \boldsymbol{e}_L} = -\sum_{k=1}^{3} (\boldsymbol{d}_L \cdot \boldsymbol{u}_k)\boldsymbol{u}_k\,, \tag{28}$$

where

$$\frac{\partial W}{\partial \boldsymbol{e}_L} = \frac{\partial W}{\partial e}\boldsymbol{g} + \frac{1}{e}\left([\boldsymbol{I} - (\boldsymbol{g} \otimes \boldsymbol{g})]^T \frac{\partial W}{\partial \boldsymbol{g}}\right). \tag{29}$$

The electric field in the deformed configuration can simply be expressed by

$$\boldsymbol{d} = -\sum_{k=1}^{3} \lambda_k (\boldsymbol{d}_L \cdot \boldsymbol{u}_k)\boldsymbol{v}_k\,. \tag{30}$$

5 Strain energy prototype

In this section, a prototype total energy function W is proposed. A more general, but complex form of the total energy function can be constructed following the work of Shariff [34], if required. We propose

$$W = W_{(T)} + W_{(\Lambda)} + W_{(E)}\,, \tag{31}$$

where

$$W_{(T)} = \mu \sum_{i=1}^{3} r_1^2(\lambda_i) + 2\mu_1 \sum_{i=1}^{3} \alpha_i r_2^2(\lambda_i) + \frac{\kappa_1}{2}\Big(\sum_{i=1}^{3} \alpha_i r_3(\lambda_i)\Big)^2\,, \tag{32}$$

$$W_{(\Lambda)} = 2\mu_2 \rho^2 \sum_{i=1}^{3} \beta_i r_4^2(\lambda_i) + \frac{\kappa_2}{2}\rho^4 \Big(\sum_{i=1}^{3} \beta_i r_5(\lambda_i)\Big)^2 + \kappa_3 \rho^2 \Big[\sum_{i=1} \alpha_i r_6(\lambda_i)\Big]\Big[\sum_{i=1}^{3} \beta_i r_7(\lambda_i)\Big]\,, \tag{33}$$

and [34]

$$W_{(E)} = \sum_{i=1}^{3} \gamma_i c_0(e) r_8^2(\lambda_i) - \varepsilon_0 \gamma_i \frac{e^2}{2\lambda_i^2}\,, \tag{34}$$

with the properties [31]

$$c_0(0) = 0\,, \quad r_\alpha(1) = 0\,, \quad r'_\alpha(1) = 1\,, \quad \alpha = 1, 2, \ldots 8\,. \tag{35}$$

We note that $\mu, \mu_1, \mu_2, \kappa_1, \kappa_2, \kappa_3$ and $c_0(e)$ are ground-state constants and their restrictions are given in Appendix A. We could also include the following property, when appropriate, r_α to represent physical strain measures with the extreme deformation values

$$r_\alpha(\lambda_i \to \infty) = \infty\,, \quad r_\alpha(\lambda \to 0) = -\infty\,. \tag{36}$$

The energy functions (31) to (34) can be easily extended to construct a more general strain energy function (see for example [31]), but the total energy function proposed in this Section should suffice to illustrate our model. From the above and Eqn. (17), it is clear that

$$\boldsymbol{d} = \varepsilon_0 \boldsymbol{e} - \boldsymbol{F}\frac{\partial W_{(E)}}{\partial \boldsymbol{e}_L} \quad \boldsymbol{p} = -\boldsymbol{F}\frac{\partial W_{(E)}}{\partial \boldsymbol{e}_L}\,. \tag{37}$$

In vacuum, $W_{(E)} = 0$ and we recover the relation

$$\boldsymbol{d} = \varepsilon_0 \boldsymbol{e}\,. \tag{38}$$

6 Boundary value problem

To illustrate our theory, we consider two simple deformations, pure bending and finite torsion of a right circular cylinder, where their displacements are known. For boundary value problems, where the displacements are unknown, the construction of solutions are described in Appendix B.

To plot the results in this section, for simplicity, we use

$$r_\alpha(x) = \ln(x)\,, \quad \alpha = 1, 2, \ldots 8\,, \tag{39}$$

and the ground-state values

$$\mu = 5\text{kPa}\,, \quad \mu_1 = 80\text{kPa}\,, \quad \kappa_1 = 0\,, \tag{40}$$

are those associated with skeletal muscle tissue [19, 27]. Since our model is new and there are no experimental values for the following ground-state constants, we use the ad hoc values

$$\mu_2 = 10.0\text{kPa}\,, \quad \kappa_1 = \kappa_2 = 0\,, \quad \kappa_3 = -100\text{kPa}\,, \quad c_0(e) = 0.1\varepsilon_0 e^2\,, \tag{41}$$

to plot the graphs. Take note that the above values satisfy the restrictions given in Appendix A.

6.1 Pure Bending

A deformation of pure bending in plane strain is depicted in Fig. 1, where a sector of a circular annulus defined by

$$r = r(x_1)\,, \quad \theta = \theta(x_2)\,, \quad z = x_3\,, \quad 0 \le x_1 \le B\,, \quad -L \le x_2 \le L\,, \quad -H \le x_3 \le H \tag{42}$$

is obtained via bending a rectangular slab of incompressible material: Note that (r, θ, z) is the cylindrical polar coordinate for the current configuration and (x_1, x_2, x_3) is the Cartesian referential coordinate with the basis $\{\boldsymbol{g}_1, \boldsymbol{g}_2, \boldsymbol{g}_3 = \boldsymbol{e}_z\}$.

The formula employed here could be used to compare our theory with experiment (for example, a three point bending test experiment described in reference [17]).

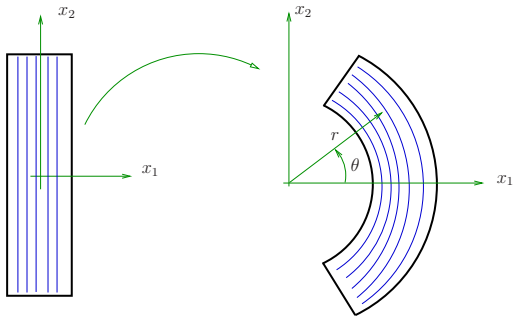

Figure 1: Bending of a rectangular block into a sector of a cylindrical tube.

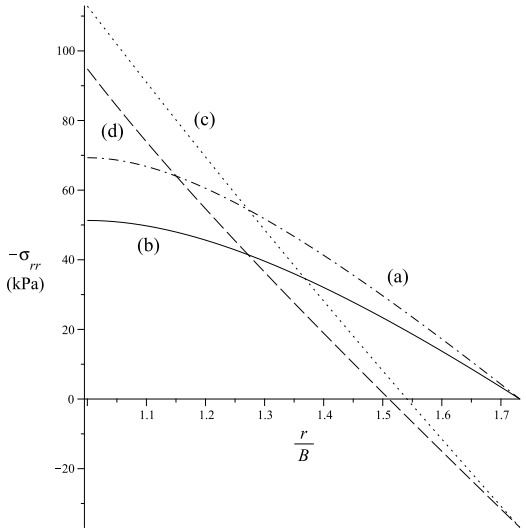

Figure 2: Radial behaviour of stress σ_{rr}. (a) Elastic solid with fibre bending resistance. $e_0 = 0$ V/m. (b) Elastic solid with no fibre bending resistance. $e_0 = 0$ V/m. (c) Elastic solid with fibre bending resistance. $e_0 = 5 \times 10^6$ V/m. (d) Elastic solid with no fibre bending resistance. $e_0 = 5 \times 10^6$ V/m.

In this case,

$$\boldsymbol{F} = r' \boldsymbol{e}_r \otimes \boldsymbol{g}_1 + r\theta' \boldsymbol{e}_\theta \otimes \boldsymbol{g}_2 + \boldsymbol{e}_z \otimes \boldsymbol{g}_3 \,. \tag{43}$$

In view of $\det \boldsymbol{F} = 1$ and the conditions $\theta(0) = 0$ and $r(A) = a$ at the boundary, we obtain

$$r^2 - a^2 = 2\chi x_1 \,, \quad \theta = \frac{x_2}{\chi} \,, \quad \chi = \frac{b^2 - a^2}{2B} > 0 \,, \tag{44}$$

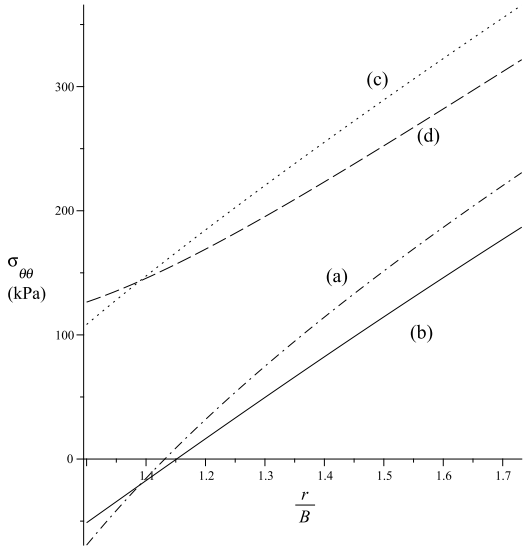

Figure 3: Radial behaviour of stress $\sigma_{\theta\theta}$.(a) Elastic solid with fibre bending resistance. $e_0 = 0$ V/m. (b) Elastic solid with no fibre bending resistance. $e_0 = 0$ V/m. (c) Elastic solid with fibre bending resistance. $e_0 = 5 \times 10^6$ V/m. (d) Elastic solid with no fibre bending resistance. $e_0 = 5 \times 10^6$ V/m.

where $r(B) = b$. Hence, in view of (3), (43) and (44), we have

$$\lambda_1 = \frac{\chi}{r}\,, \quad \lambda_2 = \frac{r}{\chi}\,, \quad \lambda_3 = 1 \tag{45}$$

and the spectral basis vectors are $\boldsymbol{u}_i = \boldsymbol{g}_i$, $\boldsymbol{v}_1 = \boldsymbol{e}_r$, $\boldsymbol{v}_2 = \boldsymbol{e}_\theta$ and $\boldsymbol{v}_3 = \boldsymbol{e}_z$.

We only study the case $\boldsymbol{a} = \boldsymbol{g}_2$ and $\boldsymbol{e} = \dfrac{e_0}{r}\boldsymbol{e}_\theta$. Hence, $\boldsymbol{e}_L = \dfrac{e_0}{\chi}\boldsymbol{g}_2$, $a_1 = a_3 = 0$, $a_2 = 1$ $c_1 = c_3 = 0$ and $c_2 = 1$ and clearly $\operatorname{Curl} \boldsymbol{e}_L = \boldsymbol{0}$ is satisfied. If we let $\bar{\boldsymbol{F}} = \boldsymbol{F}$, we get

$$\boldsymbol{k} = -\boldsymbol{g}_1\,, \quad \rho = \frac{1}{r}\,, \quad b_1 = -1\,, \quad b_2 = b_3 = 0\,. \tag{46}$$

The strain energy function is simplified, i.e.

$$\begin{aligned} W_{(T)} &= \mu \sum_{i=1}^{3} r_1^2(\lambda_i) + 2\mu_1 r_2^2(\lambda_2) + \frac{\kappa_1}{2} r_3^2(\lambda_2)\,, \\ W_{(\Lambda)} &= 2\rho^2 \mu_2 r_4^2(\lambda_1) + \rho^4 \frac{\kappa_2}{2} r_5^2(\lambda_1) + \rho^2 \kappa_3 r_6(\lambda_2) r_7(\lambda_1)\,, \\ W_{(E)} &= c_0(e) r_8^2(\lambda_2) - \frac{\varepsilon_0 e^2}{2\lambda_2^2}\,, \quad W = W_{(T)} + W_{(\Lambda)} + W_{(E)}\,. \end{aligned} \tag{47}$$

The non-zero Cauchy stress components simply becomes

$$\sigma_i = \lambda_i \frac{\partial W}{\partial \lambda_i} - p\,, \tag{48}$$

where $\sigma_1 = \sigma_{rr}$, $\sigma_2 = \sigma_{\theta\theta}$ and $\sigma_3 = \sigma_{zz}$ are cylindrical components of the Cauchy stress. The Maxwell stress simply becomes

$$\boldsymbol{T}_M = \frac{\varepsilon_0 e^2}{2r^2}(-\boldsymbol{e}_r \otimes \boldsymbol{e}_r + \boldsymbol{e}_\theta \otimes \boldsymbol{e}_\theta - \boldsymbol{e}_z \otimes \boldsymbol{e}_z)\,. \tag{49}$$

Since σ_i depends only on r, the equilibrium equation simply becomes

$$\frac{d\sigma_{rr}}{dr} + \frac{1}{r}(\sigma_{rr} - \sigma_{\theta\theta}) = 0\,. \tag{50}$$

We note that, in view of the Maxwell stress in (49), $\sigma_{rr} = -\dfrac{\varepsilon_0 e^2}{2b^2}$ at $r = b$, we then have

$$\sigma_{rr} = -\int_r^b G(y)\,dy + \frac{\varepsilon_0 e^2}{2b^2}\,, \quad rG(r) = \lambda_2\frac{\partial W}{\partial \lambda_2} - \lambda_1\frac{\partial W}{\partial \lambda_1}\,. \tag{51}$$

Hence, we can evaluate

$$p = \lambda_1\frac{\partial W}{\partial \lambda_1} + \int_r^b G(y)\,dy - \frac{\varepsilon_0 e^2}{2b^2}\,. \tag{52}$$

The stress-strain relations for $\sigma_{\theta\theta}$ and σ_{zz} can now be obtained using the above p. The bending moment

$$\mathcal{M} = \int_a^b r\sigma_{\theta\theta}\,dr \tag{53}$$

and the normal force

$$\mathcal{N} = \int_a^b \sigma_{\theta\theta} dr\,. \tag{54}$$

Both $\mathcal{M}$ and $\mathcal{N}$ are derived per unit length in the x_3 direction, and applied to a section of constant θ.

In figures 2 and 3, the behaviours of, respectively, the radial and hoop stresses are depicted using $\dfrac{\chi}{B} = 1$ and the material is deformed to $\dfrac{a}{B} = 1$. It is clear from these figures the magnitude of the stresses is affected by bending fibre resistance and by the presence of an electric field.

The bending moment $\mathcal{M}$ values are;

$$\begin{aligned}
&107.8388439 && \text{kPam}^2\,, && \text{with fibre bending resistance, } e_0 = 0 \text{ V/m}\,,\\
&80.72073233 && \text{kPam}^2\,, && \text{without fibre bending resistance } e_0 = 0 \text{ V/m}\,,\\
&252.8614021 && \text{kPam}^2\,, && \text{with fibre bending resistance, } e_0 = 5\times 10^6 \text{ V/m}\,,\\
&225.7432905 && \text{kPam}^2\,, && \text{without fibre bending resistance, } e_0 = 5\times 10^6 \text{ V/m}\,.
\end{aligned} \tag{55}$$

The normal force $\mathcal{N}$ values are;

$$\begin{aligned}
&69.32308513 && \text{kPam}\,, && \text{with fibre bending resistance, } e_0 = 0 \text{ V/m}\,,\\
&51.29533089 && \text{kPam}\,, && \text{without fibre bending resistance } e_0 = 0 \text{ V/m}\,,\\
&176.7433952 && \text{kPam}\,, && \text{with fibre bending resistance, } e_0 = 5\times 10^6 \text{ V/m}\,,\\
&158.7156409 && \text{kPam}\,, && \text{without fibre bending resistance, } e_0 = 5\times 10^6 \text{ V/m}\,.
\end{aligned} \tag{56}$$

Hence, the presence of bending fibre stiffness and an electric field increases the magnitude of $\mathcal{M}$ and $\mathcal{N}$.

We note that

$$\boldsymbol{d}_L = d_1(x_1)\boldsymbol{g}_2\,, \quad d_1(x_1) = \frac{\varepsilon_0 e}{\lambda_2^2} - c_0'(e)r_8^2(\lambda_2) \tag{57}$$

which implies that $\text{Div}\,\boldsymbol{d}_L = 0$, since the component of $\boldsymbol{d}_L$ depends on the variable x_1 only.

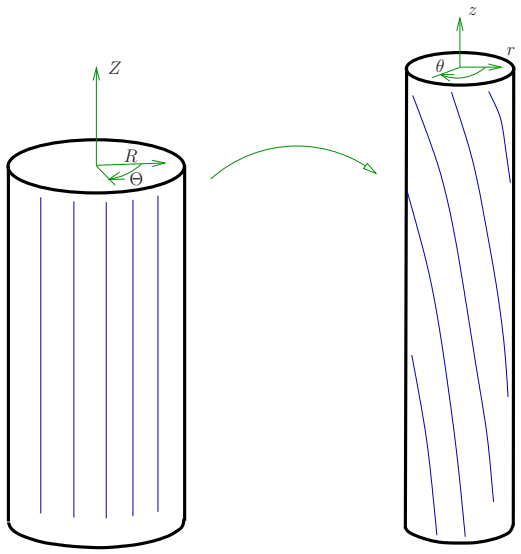

Figure 4: Torsion and extension of a cylinder

6.2 Torsion and extension of a cylinder

The initial geometry of an incompressible thick-walled circular cylindrical annulus is described by

$$0 \leq R \leq A, \quad 0 \leq \Theta \leq 2\pi, \quad 0 \leq Z \leq L, \tag{58}$$

where R, Θ and Z are reference polar coordinates with the corresponding basis $B_R = \{\boldsymbol{E}_R, \boldsymbol{E}_\Theta, \boldsymbol{E}_Z\}$. The boundary value problem illustrated here could be used in an experiment (see, for example, reference [16]) to verify our theoretical predictions.

The deformation is depicted in Fig. 4 and is described by

$$r = \lambda_z^{-\frac{1}{2}} R, \quad \theta = \Theta + \lambda_z \tau Z, \quad z = \lambda_z Z, \tag{59}$$

where τ is the amount of torsional twist per unit deformed length and λ_z is the axial stretch. In the above formulation, r, θ and z are cylindrical polar coordinates in the deformed configuration with the corresponding basis $B_C = \{\boldsymbol{e}_r, \boldsymbol{e}_\theta, \boldsymbol{e}_z\}$. Here, we have allowed $\boldsymbol{e}_r = \boldsymbol{E}_R$, $\boldsymbol{e}_\theta = \boldsymbol{E}_\Theta$ and $\boldsymbol{e}_z = \boldsymbol{E}_Z$. The deformation gradient is

$$\boldsymbol{F} = \lambda_z^{-1/2} \boldsymbol{e}_r \otimes \boldsymbol{E}_R + \lambda_z^{-1/2} \boldsymbol{e}_\theta \otimes \boldsymbol{E}_\Theta + \lambda_z \gamma \boldsymbol{e}_\theta \otimes \boldsymbol{E}_Z + \lambda_z \boldsymbol{e}_z \otimes \boldsymbol{E}_Z \,, \tag{60}$$

where $\gamma = r\tau$ and in this paper, we only consider $\lambda_z \geq 1$. The Lagrangian principal directions are:

$$\boldsymbol{u}_1 = \boldsymbol{E}_R \,, \quad \boldsymbol{u}_2 = c\boldsymbol{E}_\Theta + s\boldsymbol{E}_Z \,, \quad \boldsymbol{u}_3 = -s\boldsymbol{E}_\Theta + c\boldsymbol{E}_Z \,, \tag{61}$$

where

$$c=\cos(\phi)=\frac{2}{\sqrt{2(\hat{\gamma}^2+4)+2\hat{\gamma}\sqrt{\hat{\gamma}^2+4}}},\quad s=\sin(\phi)=\frac{\hat{\gamma}+\sqrt{\hat{\gamma}^2+4}}{\sqrt{2(\hat{\gamma}^2+4)+2\hat{\gamma}\sqrt{\hat{\gamma}^2+4}}}, \tag{62}$$

with

$$\frac{\pi}{4}\leq\frac{\pi-\tan^{-1}\left(\frac{1}{\sqrt{\lambda_z^3-1}}\right)}{2}\leq\phi<\frac{\pi}{2}\,,\quad\hat{\gamma}=\frac{\lambda_z^3\gamma^2+\lambda_z^3-1}{\lambda_z^{\frac{3}{2}}\gamma}\geq 0\,,\quad c^2-s^2=-\hat{\gamma}cs\,. \tag{63}$$

In the case of pure torsion, $\lambda_z=1$ and we have $\hat{\gamma}=\gamma$. The principal stretches for a combined extension and torsion deformation are

$$\lambda_1=\frac{1}{\lambda_z^{\frac{1}{2}}}\,,\quad\lambda_2=\sqrt{\frac{1}{\lambda_z}+\frac{s\gamma\sqrt{\lambda_z}}{c}}\,,\quad\lambda_3=\sqrt{\frac{1}{\lambda_z}-\frac{c\gamma\sqrt{\lambda_z}}{s}}. \tag{64}$$

In this section, for simplicity, we only consider the cases when $\boldsymbol{a}=\boldsymbol{E}_z$ and $\boldsymbol{e}_L=e\boldsymbol{E}_R$, where e is a

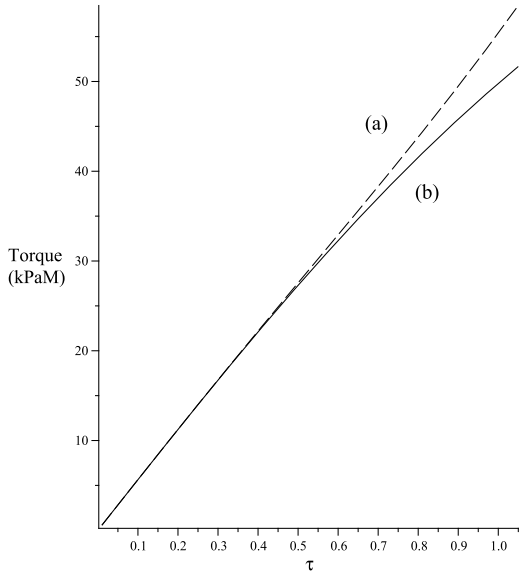

Figure 5: Torque, $\mathcal{M}$ vs τ. (a) Elastic solid with fibre bending stiffness. (b) Elastic solid with no fibre bending stiffness. $\lambda_z=1.5$. The torque is independent of the electric field $\boldsymbol{e}_L=e\boldsymbol{E}_R$.

constant. Hence, $a_1=0$, $a_2=s$, $a_3=c$, $c_2=c_3=0$ and $c_1=1$. Clearly, the relation $\mathrm{Curl}\,\boldsymbol{e}_L=0$ is satisfied. If we let $\bar{\boldsymbol{F}}=\boldsymbol{F}$ and using

$$\mathrm{Grad}\,\boldsymbol{b}=\frac{\partial\boldsymbol{b}}{\partial R}\otimes\boldsymbol{E}_R+\frac{1}{R}\frac{\partial\boldsymbol{b}}{\partial\Theta}\otimes\boldsymbol{E}_\Theta+\frac{\partial\boldsymbol{b}}{\partial Z}\otimes\boldsymbol{E}_Z\,, \tag{65}$$

we obtain

$$\boldsymbol{k}=-\boldsymbol{E}_R\,,\quad\rho=\frac{\lambda_z^3\gamma\tau}{\sqrt{\lambda_z^2(1+\gamma^2)}}\,,\quad b_1=-1\,,\quad b_2=b_3=0\,. \tag{66}$$

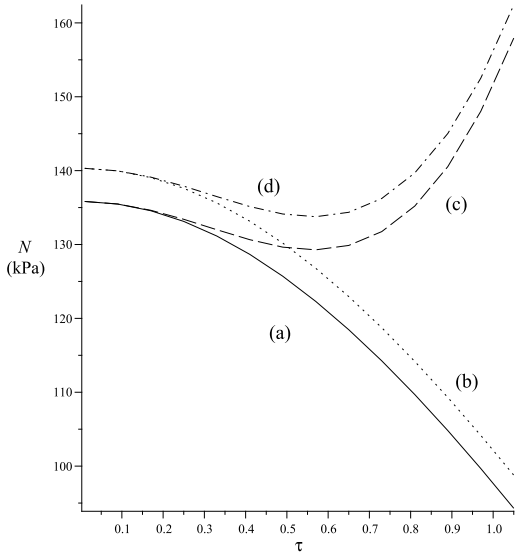

Figure 6: Force per unit area N vs τ. (a) Elastic solid without fibre bending resistance. $e = 0$ V/m. (b) Elastic solid without fibre bending resistance. $e = 5 \times 10^6$ V/m. (c) Elastic solid with fibre bending resistance. $e = 0$ V/m. (d) Elastic solid with fibre bending resistance. $e = 5 \times 10^6$ V/m. $\lambda_z = 1.5$

The strain energy function then takes the form

$$\begin{aligned} W_{(T)} &= \mu \sum_{i=1}^{3} r_1^2(\lambda_i) + 2\mu_1[s^2 r_2^2(\lambda_2) + c^2 r_2^2(\lambda_3)] + \frac{\kappa_1}{2}[s^2 r_3(\lambda_2) + c^2 r_3(\lambda_3)]^2 \,, \\ W_{(\Lambda)} &= 2\rho^2 \mu_2 r_4^2(\lambda_1) + \rho^4 \frac{\kappa_2}{2} r_5^2(\lambda_1) + \rho^2 \kappa_3 [s^2 r_6(\lambda_2) + c^2 r_6(\lambda_3)] r_7(\lambda_1) \,, \\ W_{(E)} &= c_0(e) r_8^2(\lambda_1) - \frac{\varepsilon_0 e^2}{2\lambda_1^2} \,. \end{aligned} \tag{67}$$

The Maxwell stress

$$\boldsymbol{T}_M = \frac{\varepsilon_0 \lambda_z e^2}{2} (\boldsymbol{e}_r \otimes \boldsymbol{e}_r - \boldsymbol{e}_\theta \otimes \boldsymbol{e}_\theta + \boldsymbol{e}_z \otimes \boldsymbol{e}_z) \,. \tag{68}$$

The total Cauchy stress

$$\boldsymbol{T} = 2\boldsymbol{F} \frac{\partial W}{\partial \boldsymbol{C}} \boldsymbol{F}^T - pI \,. \tag{69}$$

In view of $\boldsymbol{a} \equiv [0, 0, 1]^T$, we have $a_1 = 0$, $a_2 = s$ and $a_3 = c$ and

$$\boldsymbol{T} = \sigma_{rr} \boldsymbol{e}_r \otimes \boldsymbol{e}_r + \sigma_{\theta\theta} \boldsymbol{e}_\theta \otimes \boldsymbol{e}_\theta + \sigma_{zz} \boldsymbol{e}_z \otimes \boldsymbol{e}_z + \sigma_{z\theta} (\boldsymbol{e}_z \otimes \boldsymbol{e}_\theta + \boldsymbol{e}_\theta \otimes \boldsymbol{e}_z) \,, \tag{70}$$

where

$$\begin{aligned} \sigma_{\theta\theta} &= 2\left[\frac{l_2 c^2 + l_3 s^2 - 2 l_4 cs}{\lambda_z} + 2\sqrt{\lambda_z}\gamma((l_2 - l_3)cs + l_4(c^2 - s^2)) + \lambda_z^2 \gamma^2 (l_2 s^2 + l_3 c^2 + 2 l_4 cs) \right] - p, \\ \sigma_{z\theta} &= 2\left[\sqrt{\lambda_z}((l_2 - l_3)cs + l_4(c^2 - s^2)) + \lambda_z^2 \gamma (l_2 s^2 + l_3 c^2 + 2 l_4 cs) \right], \\ \sigma_{zz} &= 2\lambda_z^2 \left(l_2 s^2 + l_3 c^2 + 2 l_4 cs \right) - p \,, \quad \sigma_{rr} = \frac{2 l_1}{\lambda_z} - p \,, \end{aligned} \tag{71}$$

where

$$l_i = \left(\frac{\partial W}{\partial \boldsymbol{C}}\right)_{ii}, \quad i = 1,2,3\,, \quad l_4 = \left(\frac{\partial W}{\partial \boldsymbol{C}}\right)_{23}. \tag{72}$$

The normal force per unit deformed area N and the torque per unit deformed area $\mathcal{M}$ applied at the ends of the cylinder are as follows:

$$N = \frac{2}{a^2}\int_0^a \sigma_{zz} r\,\mathrm{d}r\,, \quad \mathcal{M} = \frac{2}{a^2}\int_0^a \sigma_{z\theta} r^2\,\mathrm{d}r\,, \quad a = \frac{A}{\sqrt{\lambda_z}}\,. \tag{73}$$

To remove p in $(73)_1$, we use the equilibrium relation

$$\sigma_{rr} + \sigma_{\theta\theta} = \frac{1}{r}\frac{\mathrm{d}(r^2\sigma_{rr})}{\mathrm{d}r}\,. \tag{74}$$

and re-expressed $(73)_1$ as

$$N = \frac{1}{a^2}\int_0^a (2\sigma_{zz} - \sigma_{rr} - \sigma_{\theta\theta}) r\,\mathrm{d}r + \frac{\varepsilon_0 \lambda_z e^2}{2}\,. \tag{75}$$

It is clear from Fig. 5 that, for an axial stretch $\lambda_z = 1.5$, we require more torque to twist an elastic solid cylinder with fibre bending stiffness and the torque is independent of the electric field $\boldsymbol{e}_L = e\boldsymbol{E}_R$. However, in the case of the normal force (see Fig. 6), the presence of an electric field and fibre bending stiffness, increases the magnitude of the normal force and changes its behaviour.

Since $W_{(E)}$ depends only on the constant principal stretch λ_1 (see Eqn. $(67)_3$), it is clear that the property $\mathrm{Div}\,\boldsymbol{d}_L = 0$ is satisfied.

7 Conclusion

We have modelled elastic resistance due to changes in the curvature of the fibres without using the second gradient theory. In view of this, our proposed constitutive equation is simpler (as shown in Sections 4 and 5) than the second-gradient constitutive equations given in the literature; solving boundary value problems using our model is also simpler as exemplified in Section 6. Our model does not contain contact torques (which is required in a second gradient model) and hence the proposed model is more realistic in the sense that contact torques do not exist in deformations of non-polar carbon fiber-reinforced EAPs. Our constitutive equation uses recently developed spectral invariants (see Section 4.1) that are attractive and useful for experimental designs. The boundary value problem results in Section 6 indicate that our model manage to simulate fibre bending stiffness. In the near future, stable numerical decoupling strategies will be developed, whereas a level set description can be used to model the fibre direction [12, 13, 14]. FEM solutions of the proposed model will be obtained and we will extend this model to EAPs that are reinforced with a family of two fibres.

Acknowledgment

AL gratefully acknowledges the financial support of KU through grant FSU-2021-027.

Appendix A

The importance of strong ellipticity is explained in [22]. In this paper, we restrict the material constants given in Section 5 using the following strong ellipticity condition in the incompressible reference configuration ($\boldsymbol{F} = I$) [22]:

Let $\boldsymbol{m}$ and $\boldsymbol{n}$ be unit vectors with the condition $\boldsymbol{m}\cdot\boldsymbol{n}=0$ [22]. The strong ellipticity condition

$$\boldsymbol{m}\cdot[\boldsymbol{Q}(\boldsymbol{n})\boldsymbol{m}]>0\,, \tag{A1}$$

where the Cartesian components of $\boldsymbol{Q}(\boldsymbol{n})$ are

$$(\boldsymbol{Q}(\boldsymbol{n}))_{ij}=\sum_{p,q=1}^{3}\left(\frac{\partial^2 W}{\partial \boldsymbol{F}^2}\right)_{piqj} n_p n_q\,, \tag{A2}$$

and n_i is a Cartesian component of $\boldsymbol{n}$. Following the work of Shariff et al. [29], in view of (A2) and (31), we obtain

$$\boldsymbol{Q}(\boldsymbol{n})=\boldsymbol{Q}_1(\boldsymbol{n})+\boldsymbol{Q}_2(\boldsymbol{n})+\boldsymbol{Q}_3(\boldsymbol{n})+\boldsymbol{Q}_4(\boldsymbol{n})+\boldsymbol{Q}_5(\boldsymbol{n})\,, \tag{A3}$$

where

$$\begin{aligned}
\boldsymbol{Q}_1(\boldsymbol{n}) &= \mu(\boldsymbol{I}+\boldsymbol{n}\otimes\boldsymbol{n})+k_1\boldsymbol{A}\boldsymbol{n}\otimes\boldsymbol{A}\boldsymbol{n}+\mu_1(\boldsymbol{A}\boldsymbol{n}\otimes\boldsymbol{n}+\boldsymbol{n}\otimes\boldsymbol{A}\boldsymbol{n}+(\boldsymbol{n}\cdot\boldsymbol{A}\boldsymbol{n})\boldsymbol{I}+\boldsymbol{A})\,,\\
\boldsymbol{Q}_2(\boldsymbol{n}) &= k_2\rho^2(\boldsymbol{K}\boldsymbol{n}\otimes\boldsymbol{K}\boldsymbol{n})+k_3\rho^2(\boldsymbol{A}\boldsymbol{n}\otimes\boldsymbol{K}\boldsymbol{n}+\boldsymbol{K}\boldsymbol{n}\otimes\boldsymbol{A}\boldsymbol{n})\,,\\
\boldsymbol{Q}_3(\boldsymbol{n}) &= \mu_2\rho^2(\boldsymbol{K}\boldsymbol{n}\otimes\boldsymbol{n}+\boldsymbol{n}\otimes\boldsymbol{K}\boldsymbol{n}+(\boldsymbol{n}\cdot\boldsymbol{K}\boldsymbol{n})\boldsymbol{I}+\boldsymbol{K})\,,\\
\boldsymbol{Q}_4(\boldsymbol{n}) &= \frac{c_0(e)}{2}[\boldsymbol{G}\boldsymbol{n}\otimes\boldsymbol{n}+\boldsymbol{n}\otimes\boldsymbol{G}\boldsymbol{n}+(\boldsymbol{n}\cdot\boldsymbol{G}\boldsymbol{n}))\boldsymbol{I}+\boldsymbol{G}]\,,\\
\boldsymbol{Q}_5(\boldsymbol{n}) &= -\epsilon_0 e^2(\boldsymbol{n}\otimes\boldsymbol{G}\boldsymbol{n}+\boldsymbol{G}\boldsymbol{n}\otimes\boldsymbol{n}+\boldsymbol{G})\,,
\end{aligned} \tag{A4}$$

$$\boldsymbol{A}=\boldsymbol{a}\otimes\boldsymbol{a}\,,\quad \boldsymbol{K}=\boldsymbol{k}\otimes\boldsymbol{k}\,,\quad \boldsymbol{G}=\boldsymbol{g}\otimes\boldsymbol{g}\,. \tag{A5}$$

We only consider the case for $\boldsymbol{m}$ and $\boldsymbol{n}$ in a plane, since in Section 6, the boundary value problems can be considered as two dimensional. In view that at $\boldsymbol{F}=\boldsymbol{I}$, $\boldsymbol{u}_i$ is arbitrary, we assume $\boldsymbol{u}_i=\boldsymbol{g}_i$.

If we consider a material, where $k_1=k_2=k_3=0$, the necessary and sufficient condition for (A1) is

$$b_1>0\quad\text{and}\quad 4b_1b_2>b_3\,, \tag{A6}$$

where

$$\begin{aligned}
b_1 &= \mu+\mu_1(\alpha_1+\alpha_2)+\mu_2\rho^2(\beta_1+\beta_2)+\frac{c_0(e)}{2}(\gamma_1+\gamma_2)-\varepsilon_0 e^2\gamma_2\,,\\
b_2 &= \mu+\mu_1(\alpha_1+\alpha_2)+\mu_2\rho^2(\beta_1+\beta_2)+\frac{c_0(e)}{2}(\gamma_1+\gamma_2)-\varepsilon_0 e^2\gamma_1\,,\\
b_3 &= 2\epsilon_0 e^2 c_1 c_2\,.
\end{aligned} \tag{A7}$$

In the case where k_1, k_2 and k_3 have none zero values, the inequalities

$$k_1>0\,,\quad k_1k_2\rho^2-k_3^2\rho^4>0 \tag{A8}$$

and those given (A6) ensure that (A1) is satisfied.

Appendix B

Let $\boldsymbol{d}_\alpha$, $\alpha=0,1,\ldots$ be approximate values of $\boldsymbol{d}$ that are obtained via the description below. If the deformation is not known, as a first iteration, we first solve the boundary value problem (BVP) using

$$W=W_{(T)}+W_{(E)} \tag{B1}$$

and this boundary value problem solution is used to evaluate the first approximation $\boldsymbol{d}_0$. We then solve the BVP via the following iteration:
For $i = 0, 1, \ldots$
Solve the BVP using $\boldsymbol{d}_i$ and

$$W = W_{(T)} + W_{(\Lambda)} + W_{(E)}\,. \tag{B2}$$

Obtain $\boldsymbol{d}_{i+1}$ from the solution of the BVP.
If $\|\boldsymbol{d}_{i+1} - \boldsymbol{d}_i\| <$ tolerance. Stop. We consider this is the final solution,
else
Continue with the iteration
endif
Note that, $\| \bullet \|$ is the Euclidean norm and we assume that the above iteration converges.

Data availability

All data generated or analysed during this study are included in this published article [and its supplementary information files].

References

[1] Bar-Cohen, Y. Electro-active polymers: current capabilities and challenges. In: Proceedings of the 4th Electroactive Polymer Actuators and Devices (EAPAD) Conference, 9th Smart Structures and Materials Symposium, 2002.

[2] Cao, K., Wang, B., Ding, H., Lv, L., Dong, R., Cheng, T., Gong, F. (2021). Improving Physical Layer Security of Uplink NOMA via Energy Harvesting Jammers. *IEEE Transactions on Information Forensics and Security*, **16**, 786-799.

[3] Chukov, D., Nematulloev, S., Zadorozhnyy, M., Tcherdyntsev, V., Stepashkin, A., Zherebtsov, D. (2019). Structure, mechanical and thermal properties of polyphenylene sulfide and polysulfone impregnated carbon fiber composites. *Polymers* **11**, 684.

[4] Clyne, T.W., Hull, D. (2019). An Introduction to Composite Materials, 3rd ed.; Cambridge University Press: Cambridge, UK.

[5] Dorfmann, A., and Ogden, R.W. (2005). Nonlinear electroelasticity. **Acta Mech**, **174**, 167183.

[6] Ferreti, M., Madeo, A., Dell'isola, F., and Boisse, P. (2013). Modeling the onset of shear boundary layers in fibrous composite reinforcements by second gradient theory. *Zeitschrift fur Angewandte Mathematik und Physik*, **65(3)**, 587- 612

[7] Gizzi, A., Ruiz-Baier, R., Rossi, S., Laadhari, A., Cherubini, C., Filippi, S. (2015). A three-dimensional continuum model of active contraction in single cardiomyocytes. *Cham: Springer International Publishing.* 157-176. https://doi.org/10.1007/978-3-319-05230-4_6.

[8] Hadjesfandiari, A.R., Dargush, G.F.(2011). Couple stress theory for solids. *Int. J. Solids Struct.* **48**, 2496- 2510.

[9] Hadjesfandiari, A.R., DargushG.F. (2015). Evolution of generalized couple-stress continuum theories:a critical analysis. PreprintarXiv:1501.03112.

[10] Huang, Z., Luo, P., Zheng, H., Lyu, Z., Ma, X. (2023). Novel one-dimensional V3S4@NC nanofibers for sodium-ion batteries. *Journal of Physics and Chemistry of Solids*, **172**, 111081.

[11] Kovetz, A. (2000). Electromagnetic theory. Oxford: Oxford University Press.

[12] Laadhari, A., Székely, G. (2016). Eulerian finite element method for the numerical modeling of fluid dynamics of natural and pathological aortic valves. *J. Comput. Appl. Math.* **319**, 236 - 261. https://doi.org/10.1016/j.cam.2016.11.042.

[13] Laadhari, A., Székely, G. (2017). Fully implicit finite element method for the modeling of free surface flows with surface tension effect. *Int. J. Numer. Methods Eng.* **111(11)**, 1047 - 1074.

[14] Laadhari, A. (2018). Implicit finite element methodology for the numerical modeling of incompressible two-fluid flows with moving hyperelastic interface. *Appl. Math. Comput* **333**, 376 - 400.

[15] Linul, E., Lell, D., Movahedi, N., Codrean, C., Fiedler, T. (2019). Compressive properties of Zinc Syntactic Foams at elevated temperatures. *Compos. Part B Eng.*, **167**, 122 - 134.

[16] Lu, W-Y., Jin, H., Foul, J.W., Ostien, J., Kramer, S.L., Jones, A. (2021). Solid cylinder torsion for large shear deformation and failure of engineering materials. *Experimental Mechanics*, **61**, 307- 320.

[17] Mathieu, S., Hamila, N., Bouillon, F. Boisse, P. (2015). Enhanced modeling of 3D composite preform deformations taking into account local fiber bending stiffness. *Composites Science and Technology*, **117**, 322 - 333.

[18] Monteiro, S.N., de Assis, F.S., Ferreira, C.L., Simonassi, N.T., Weber, R.P., Oliveira, M.S., Colorado, H.A., Pereira, A.C. (2018). Fique fabric: A promising reinforcement for polymer composites. *Polymers*, **10**, 246.

[19] Morrow, D. A. , Donahue, T. L. H. , Odegard, G. M. , Kaufman, K. R. (2010). Transversely isotropic tensile material properties of skeletal muscle tissue. *Journal of the Mechanical Behavior of Biomedical Materials*, **3** , 124 - 129 .

[20] Movahedi, N., Linul, E. (2017). Quasi-static compressive behavior of the ex-situ aluminum-alloy foam-filled tubes under elevated temperature conditions. *Mater. Lett.*, **206**, 182 - 184.

[21] Neff, P., Münch, I., Ghiba, I., Madeo, A. (2016). On some fundamental misunderstandings in the indeterminate couple stress model. A comment on recent papers of A.R. Hadjesfandiari and G.F. Dargush. *Int. J. Solids Struct.* **81**, 233 - 243.

[22] Ogden, R.W. (1984). Non-linear elastic deformations. Chichester: Ellis Horwood.

[23] Ogden, R.W., Steigmann, D.J. (2011). Mechanics and electrodynamics of magneto- and electro-elastic materials. (CISM Courses and Lectures Series, vol. 527). Wien: Springer.

[24] Pipkin, A.C. (1979). Stress analysis for fiber-reinforced materials. *Advances in Applied Mechanics*, **19**, 151.

[25] Shariff, M. H. B. M. (2012). Physical invariant strain energy function for passive myocardium. *Journal of Biomechanics and Modeling in Mechanobiology*, **12 (2)**, 215 - 223 .

[26] Shariff, M. H. B. M. (2016). Anisotropic separable free energy functions for elastic and non-elastic solids. *Acta Mech.*, **227(11)**, 3213 -3237.

[27] Shariff, M/H.B.M. (2017). On the spectral constitutive modelling of transversely isotropic soft tissue: Physical invariants. *International Journal of Engineering Science*, **120**, 199 - 219.

[28] Shariff, M. H. B. M. and Merodio, J. (2020). Residually stressed fiber reinforced solids: a spectral approach. *Materials*, **13(18)**, 4076.

[29] Shariff, M.H.B.M., Bustamante, R., Merodio, J. (2020). A nonlinear electro- elastic model with residual stresses and a preferred direction, *Mathematics and Mechanics of Solids*, **25 (3)**, 838-865.

[30] Shariff, M.H.B.M., Bustamante, R., Merodio, J. (2020). A nonlinear con- stitutive model for a two preferred direction electro-elastic body with residual, *International Journal of Non-Linear Mechanics*, **119**, 103352, https://doi.org/10.1016/j.ijnonlinmec.2019.103352.

[31] Shariff, M.H.B.M. (2022). A generalized strain approach to anisotropic elasticity. *Scientific reports*, **12 (1)**, 1-22.

[32] Shariff, M.H.B.M., Merodio, J., Bustamante, R. (2022). Shariff, M. H. B. M. and Merodio, J. and Bustamante, R. (2022) Finite deformations of fibre bending stiffness: A spectral approach. *Journal of Applied and Computational Mechanics*, **8(4)**, 1332-1342.

[33] Shariff, M.H.B.M., Merodio, J., Bustamante, R. (2022). Nonlinear elastic constitutive relations of residually stressed composites with stiff curved fibres. *Applied Mathematics and Mechanics* **43 (10)** , 1515 - 1530.

[34] Shariff, M.H.B.M. (2022). A generalized strain approach to anisotropic elasticity, *Scientic Reports*, **12 (1)**, 1- 22.

[35] Shariff, M.H.B.M. (2023). On the Smallest Number of Functions Representing Isotropic Functions of Scalars, Vectors and Tensors. *The Quarterly Journal of Mechanics and Applied Mathematics*, https://doi.org/10.1093/qjmam/hbac022.

[36] Shariff, M.H.B.M., Bustamante, R., Hossain, M. (2023). A Generalised Time-Dependent Mathematical Formulation for Magnetoelectrically Coupled Soft Solids at Finite Strains. *Symmetry*, **15 (3)**, 628.

[37] Shariff, M.H.B.M., Merodio, J. and Bustamante, R. (2023). A nonsecondgradient model for nonlinear elastic bodies with fibre stiffness, *Scientific Reports*, **13:6562**, https://doi.org/10.1038/s41598-023-33670-6.

[38] Sherif, G., Chukov, D., Tcherdyntsev, V., Torokhov, V. (2019). Effect of formation route on the mechanical properties of the polyethersulfone composites reinforced with glass fibers. *Polymers*, **11**, 1364.

[39] Shi, M., Wang, R., Li, L., Chen, N., Xiao, P., Yan, C., Yan, X. (2022). Redox-Active Polymer Integrated with MXene for Ultra-Stable and Fast Aqueous Proton Storage. *Adv. Funct. Mater.*, **33**, 2209777.

[40] Soldatos, K.P., Shariff, M.H.B.M., Merodio, J. (2020). On the Constitution of Polar Fibre-reinforced Materials, *Mech. Adv. Mater. Struct.*, 28(21), 2255 - 2266.

[41] Song, Z.; Shao, X.; Wu, W.; Liu, Z.; Yang, M.; Liu, M.; Wang, H. (2023). Structures and Stabilities of Carbon Chain Clusters Influenced by Atomic Antimony. *Molecules*, **28**, 1358.

[42] Spencer, A.J.M. and Soldatos, K.P. (2007). Finite deformations of fibre-reinforced elastic solids with fibre bending stiffness. *International Journal of Non-Linear Mechanics*, **42**, 355 - 368.

[43] Spencer, A.J.M. (1972). Deformations of Fibre-Reinforced Materials, Oxford University Press, 1972.

[44] Steigmann, D. (2012). Theory of elastic solids reinforced with fibers resistant to extension, flexure and twist. *Int. Jou. of Non-Linear Mechanics*, **47**, 734 - 742.

[45] Wu, Z., Lin, B., Fan, J., Zhao, J., Zhang, Q., Li, L. (2022). Effect of Dielectric Relaxation of Epoxy Resin on Dielectric Loss of Medium-Frequency Transformer. *IEEE Transactions on Dielectrics and Electrical Insulation*, **29 (5)**, 1651-1658.

[46] Xiao, X., Zhang, Q., Zheng, J., Li, Z., Yan, X. (2023). Analytical model for the nonlinear buckling responses of the confined polyhedral FGP-GPLs lining subjected to crown point loading. *Engineering Structures*, **282**, 115780.

[47] Yashas Gowda, T.G., Sanjay, M.R., Subrahmanya Bhat, K., Madhu, P., Senthamaraikannan, P., Yogesha, B. (2018). Polymer matrix-natural fiber composites: An overview. *Cogent. Eng.* **5**, 1446667.

[48] Zagho, M.M., Hussein, E.A., Elzatahry, A.A. (2018). Recent overviews in functional polymer composites for biomedical applications. *Polymers*, **10**, 739.

Author contributions

M.H.B.M.S Writing-original draft, Writing-review, and editing. All authors reviewed the manuscript.